NANO · MICRO small
www.small-journal.com

High Performance Air Breathing Flexible Lithium–Air Battery

*Ahmad Jaradat, Chengji Zhang, Sachin Kumar Singh, Junaid Ahmed, Alireza Ahmadiparidari, Leily Majidi, Sina Rastegar, Zahra Hemmat, Shuxi Wang, Anh T. Ngo, Larry A. Curtiss, Matthew Daly, Arunkumar Subramanian, and Amin Salehi-khojin**

Lithium–oxygen ($Li–O_2$) batteries possess the highest theoretical energy density (3500 Wh kg^{-1}), which makes them attractive candidates for modern electronics and transportation applications. In this work, an inexpensive, flexible, and wearable $Li–O_2$ battery based on the bifunctional redox mediator of $InBr_3$, MoS_2 cathode catalyst, and Fomblin-based oxygen permeable membrane that enable long-cycle-life operation of the battery in pure oxygen, dry air, and ambient air is designed, fabricated, and tested. The battery operates in ambient air with an open system air-breathing architecture and exhibits excellent cycling up to 240 at the high current density of 1 A g^{-1} with a relative humidity of 75%. The electrochemical performance of the battery including deep-discharge capacity, and rate capability remains almost identical after 1000 cycle in a bending fatigue test. This finding opens a new direction for utilizing high performance $Li–O_2$ batteries for applications in the field of flexible and wearable electronics.

1. Introduction

Flexible and lightweight energy storage systems are emerging as a promising technology for stretchable and wearable devices with applications in health monitoring and diagnostics,[1–5] human–machine interface devices,[6,7] cell phones and laptops,[8,9] internet of things,[10] and athletics applications.[11,12] Among various alternative energy storage systems, Li–Oxygen ($Li–O_2$) batteries are promising candidates to meet the requirements of modern flexible electronics with a long-time operation due to their ultrahigh theoretical energy density of ≈3500 Wh kg^{-1} which is about one order of magnitude higher than that of Li-ion batteries (≈400 Wh kg^{-1}).[13–15] However, most flexible $Li–O_2$ batteries operate with a current density in the range of 100–500 mA g^{-1},[16–25] which is far from practical applications of flexible electronics. In addition, the majority of these batteries operate in a pure oxygen environment. Thus, it is imperative that these batteries operate at much higher current rates in an air-like atmosphere since it enables a much higher volumetric energy density compared to its operation in a pure oxygen environment. It also provides a safe and cost-effective approach. Nevertheless, in the presence of all components of air (e.g., nitrogen (N_2), carbon dioxide (CO_2), and moisture), the $Li–O_2$ battery operation becomes more complex and serious issues are imposed on the battery including: i) degradation of anode due to its reaction with air compounds, ii) clogging of the cathode due to formation of poorly reversible side products such as lithium hydroxide (LiOH), and iii) degradation of the electrolyte due to sides reactions.[26–28] These issues negatively affect the round-trip efficiency and cause other problems, such as parasitic reactions, which lead to poor cyclability and early death of the battery.[29–32]

To resolve these issues, in this study, we designed, fabricated, and tested a new architecture for sheet-type flexible $Li–O_2$ batteries that operate in ambient air with an open system (flow in and out) where unlike closed systems, no gas storage chamber is needed. In addition, our system is comprised of a Fomblin-based protection layer to filter unwanted air species, such as H_2O,[33] and an electrolyte blend of 1 M bis(trifluoromethanesulfonyl) imide (LiTFSI) salt, redox mediator (RM) of indium bromide ($InBr_3$) to simultaneously reduce the charge potential and protect the anode from parasitic reactions,[34] and dimethyl sulfoxide (DMSO) and ionic liquid of 1-Ethyl-3-methylimidazolium tetrafluoroborate EMIM-BF4

A. Jaradat, C. Zhang, S. K. Singh, A. Ahmadiparidari, L. Majidi, S. Rastegar, Z. Hemmat, S. Wang, A. Subramanian, A. Salehi-khojin
Department of Mechanical and Industrial Engineering
University of Illinois at Chicago
Chicago, IL 60607, USA
E-mail: salehikh@uic.edu

C. Zhang, A. T. Ngo, L. A. Curtiss
Materials Science Division
Argonne National Laboratory
Lemont, IL 60439, USA

J. Ahmed, M. Daly
Department of Civil and Materials Engineering
University of Illinois at Chicago
Chicago, IL 60607, USA

S. Wang
Department of Physics
University of Illinois at Chicago
Chicago, IL 60607, USA

A. T. Ngo
Department of Chemical Engineering
University of Illinois at Chicago
Chicago, IL 60608, USA

The ORCID identification number(s) for the author(s) of this article can be found under https://doi.org/10.1002/smll.202102072.

DOI: 10.1002/smll.202102072

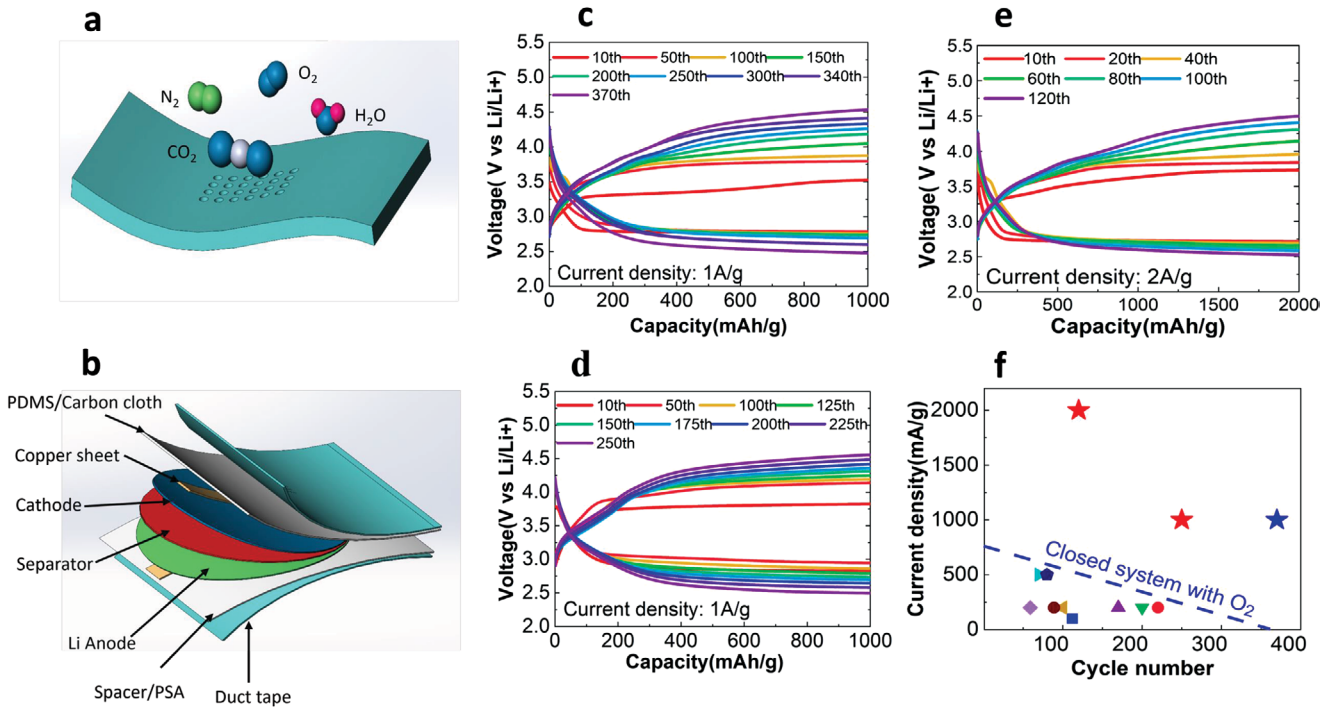

Figure 1. Schematic illustration and electrochemical performance of flexible Li–O_2 battery in oxygen and dry air. a) Schematic of flexible Li–O_2 battery. b) Multilayer structure of the battery. c) Discharge/charge curves in oxygen chamber. d,e) Discharge/charge curves at different current densities and capacities in dry air chamber. f) Comparison of current density versus cycle number of the battery in oxygen (blue star) and dry air (red stars), and other references (only available with O_2), based on 2.5 V cut-off voltage.

(9:1 volumetric ratio) that works in synergy with a 2D molybdenum disulfide (MoS_2) nanoflake (NFs) catalyst. 2D MoS_2 NFs are one of the best catalysts[35–40] for both oxygen reduction and evolution reactions occurring during discharge and charge, respectively, far exceeding the performance of Au and Pt catalysts.[41] This combination of MoS_2 catalyst and electrolyte blend was recently found to be effective in a conventional Li–O_2 system (Swagelok) which is a closed, rigid, and bulky system.[42] With such knowledge learned, in this work, we focused on design of a robust battery system that enables working under harsh conditions, such as bending/fatigue tests with an excellent structural integrity and stable electrochemical performance after 1000 bending cycles. A comprehensive study of the operation of this battery chemistry was performed in a pure oxygen, dry air, and ambient air environment (75% relative humidity).

2. Results and discussion

2.1. Flexible Battery Operating in Oxygen/Dry Air Environment

To perform the battery experiments in oxygen, dry air, and ambient air conditions, battery setups were assembled using a stack method, in which anode, separator, and cathode were stacked on top of each other as illustrated in **Figure 1**a,b (details in the Experimental Section). Figure 1c shows the charge and discharge curves in a pure oxygen environment at the current density of 1 A g^{-1}, and cut-off potentials of 2.5–4.5 V with a fixed capacity of 1000 mAh g^{-1}. The corresponding areal current density and capacity are 0.1 mA cm^{-2} and 0.1 mAh cm^{-2}, respectively. The total time for each cycle is 2 h. The charge potential at a selected cycle of 10 is ≈3.5 V which is a low value at this current density compared to >3.8 V for other works.[16–25] While charging, the Br^- gets oxidized on the cathode surface to Br_3^- which reacts with Li_2O_2 to produce Li^+ and oxygen molecules as well as regenerating the reduced form of Br_3^-.[34,43,44] Through cycling, the charge voltage reaches 4.04 V after 150 cycles and increases gradually to reach 4.5 V at 370 cycles. Figure 1d represents voltage profiles with the current density of 1 A g^{-1}, cut-off potentials of 2.5–4.5 V with a fixed capacity of 1000 mAh g^{-1} in dry air environment. Results indicate discharge and charge potentials of 2.8 and 3.8 V, respectively, at the 10th cycle. These potentials become 2.5 and 4.5 V after 250 cycles. Figure 1e displays the results obtained under 2000 mAh g^{-1} fixed capacity and doubled current density of 2 A g^{-1} in dry air environment. The battery was operated up to 120 cycles where the discharge potential reached the cut-off value. This is the first sheet-type flexible Li–O_2 battery running in dry air environment with a high current density of 2 A g^{-1}. Figure 1f illustrates a comparison between this work and other studies in the literature, demonstrating that both the current density and the cycle life are enhanced significantly.[17,18,21,22,24,25,27]

2.2. Flexible Battery Operating in Ambient Air

To operate the battery in ambient air, the carbon cloth porous membrane was soaked into Fomblin liquid chemical and

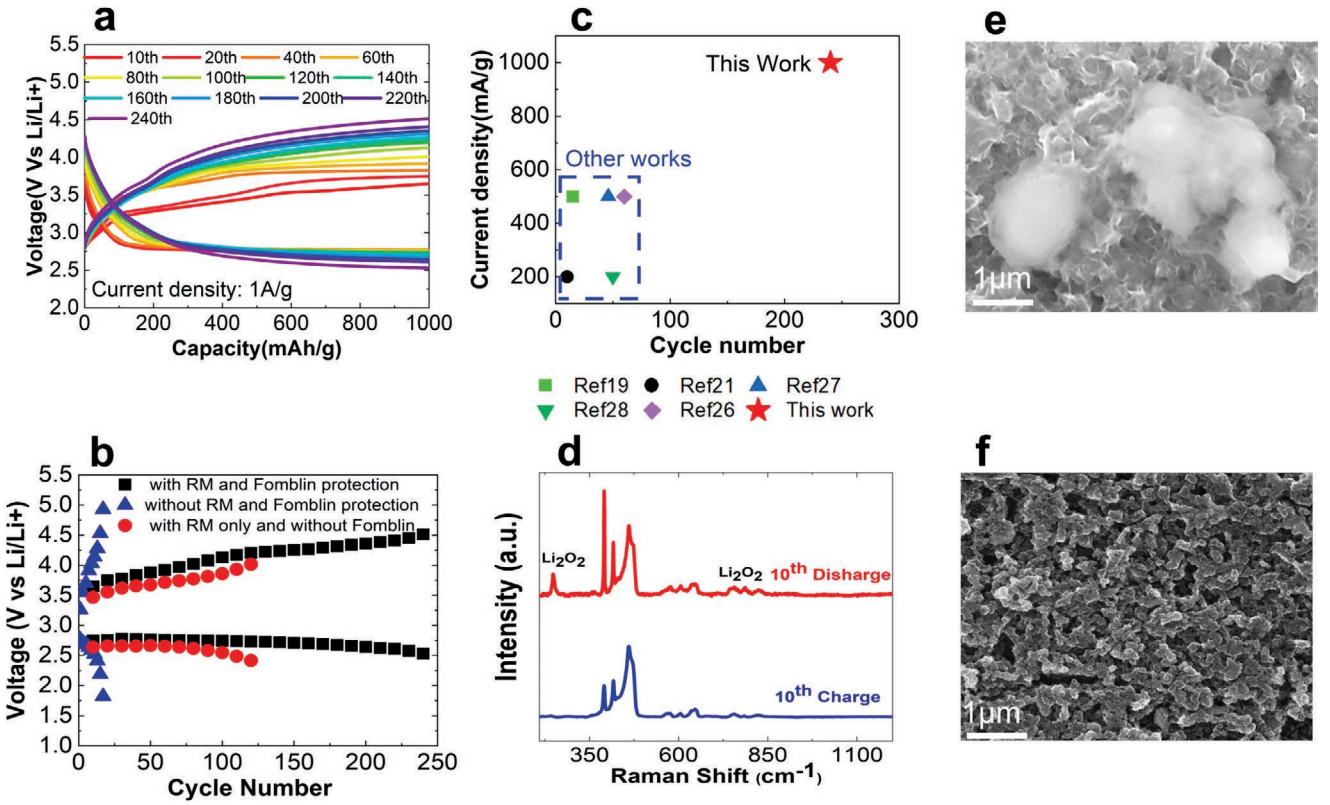

Figure 2. Electrochemical performance and morphology characterization of flexible Li–O_2 battery in ambient air. a) Discharge/charge curves of battery in ambient air. b) Cycling stability with charge and discharge voltages for control and real experiments at the current density of 1 A g^{-1}. c) Comparison of current density versus cycle number for sheet-type flexible Li–O_2 battery in ambient air for our work and other references (based on 2.5v cut-off voltage). d) Raman spectroscopy of the cathode after 10th discharge and charge cycle. e,f) SEM images of cathode surface after the 10th discharge and charge cycle, respectively.

located on the top of the cathode for filtering of humidity and other air compounds. Fomblin contains several highly flexible C—O—C chemical groups which prevent moisture and permeation of other gases and facilitate the diffusion of oxygen molecules.[33] Since the amount of redox mediator is critical for the performance of Li–air batteries, we performed optimization experiments with 100 and 30 × 10^{-3} M of $InBr_3$ and without using $InBr_3$. Results indicate that at the concentration of 100 × 10^{-3} M (shown in Figure S1a, Supporting Information), a big plateau was formed during the discharge process which leads to a reduced Li_2O_2 capacity. For instance, up to 50 cycles, the battery loses more than 30% of the discharge capacity. On the other hand, the result of the battery without using $InBr_3$ is shown in Figure S1b (Supporting Information). At the 50th cycle, the charge potential without $InBr_3$ remains above 4.25 V, while the charge potential of 3.88 V was obtained with 30 × 10^{-3} M of $InBr_3$ as shown in **Figure 2**a. Thus, the 30 × 10^{-3} M of the $InBr_3$ is the optimized concentration of the RM.

As shown in Figure 2a, with 30 × 10^{-3} M the $InBr_3$, the battery also demonstrates a long life of 240 cycles in ambient air with a relative humidity of 75% operating with a current density of 1 A g^{-1} and a fixed capacity of 1000 mAh g^{-1}. This exhibits remarkable stability of the battery in ambient air with relative humidity of 75%, especially the discharge voltage, which remains above 2.6 V in ambient air even up to 200 cycles as seen in Figure 2b. To study the role of the RM and Fomblin protection layer in ambient air environment, we performed two control experiments. First, we excluded both the Fomblin layer and RM. As shown in Figure 2b, and Figure S2a (Supporting Information), the battery failed after 16 cycles due to a drop in the discharge voltage (2.02 V). In the second step, we used the RM only and without Fomblin. As seen from Figure 2b; and Figure S2b (Supporting Information), the discharge potential dropped to 2.5 V and charge potential was increased to 3.93 after 110th cycle. The battery failed after 120 cycles. However, with both the protection layer and RM, the battery was operated up to 240 cycles. This set of results further confirms the effectiveness of utilizing both the RM and protection layer. Figure 2c illustrates a comparison between this work and other studies in the literature. Overall, the current density and cycle life achieved in this study are much higher than previously reported values.[19,21,26–28] To rule out the contribution of carbon cloth toward the battery performance, we run a control experiment using carbon cloth only (without MoS_2 catalyst). The battery failed after 45 cycles as illustrated in Figure S3 (Supporting Information). Also, to further evaluate the catalytic activity of 2D MoS_2 nanoflakes, we performed comparison experiment using MoS_2 powder during discharge and charge processes. When using MoS_2 powder, the battery failed after 40 cycles as illustrated in Figure S4 (Supporting Information).

As for characterizations of 2D MoS_2 NFs, we have utilized different techniques in our previous report, such as scanning

electron microscopy (SEM), scanning transmission electron microscopy (STEM), electron energy loss spectroscopy (EELS), X-ray photoelectron spectroscopy (XPS) to verify morphology, crystal structure, and electric properties of the material.[41] To study the discharge products, several characterization techniques were also performed on the ambient air samples. Raman spectroscopy was employed on the cathode surface after the 10th discharge and charge cycles. As shown in Figure 2d, Raman peaks observed at 250 and 787 cm^{-1} indicate the formation of Li_2O_2. Additionally, no side products (e.g., LiOH, lithium carbonate) appeared as no other Raman peaks were observed except those corresponding to the substrate (exfoliated MoS_2 nanoflakes on carbon cloth).[35] The Li_2O_2 peaks at 250 and 787 cm^{-1} disappeared after the 10th charge cycle, indicating the decomposition of Li_2O_2. For the Raman results in the oxygen environment, please see Section S1 (Supporting Information). To study the morphology and topography of the discharge product, SEM was conducted. The SEM image shown in Figure 2e reveals a cloud-like structure for the product. Figure 2f shows the cathode surface (MoS_2 catalyst) after the 10th charge cycle confirming the decomposition of Li_2O_2 product. Detailed information is available in Section S2 (Supporting Information).

Next, transmission electron microscopy (TEM) was performed at low- and high-resolution imaging conditions to examine the discharged cathode, as illustrated in **Figure 3**a,b. High-resolution TEM image in Figure 3b shows that the discharged cathode is comprised of a surface layer on top of the crystalline MoS_2 nanoflakes. The measured lattice spacing of 6.2 Å within this flake is consistent with previously reported MoS_2 interlayer spacing[44,45] (see Section S3 for details on TEM imaging, Sup-

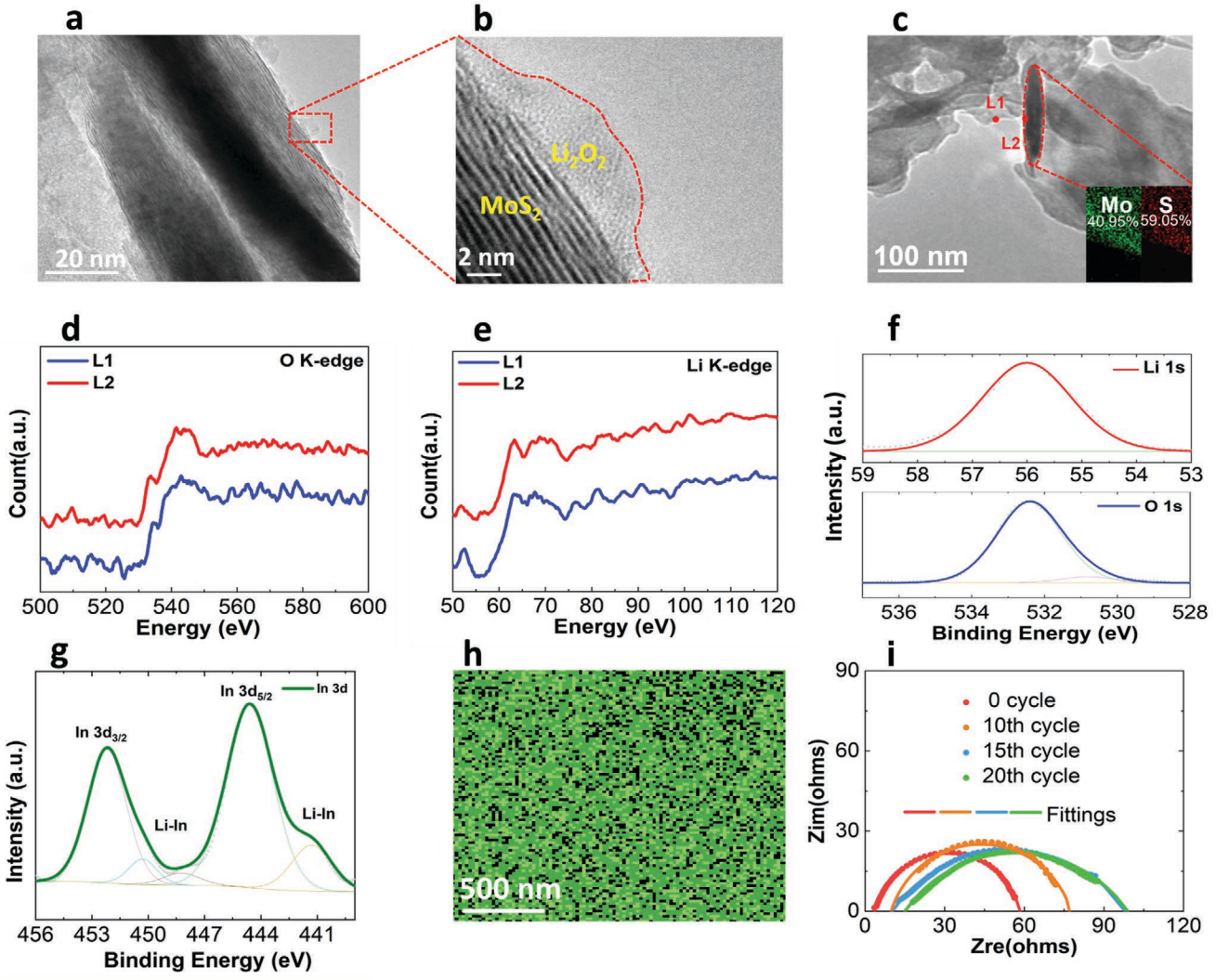

Figure 3. Elemental mapping and chemical composition characterization of Li–O_2 battery in ambient air. a,b) Low- and high-resolution TEM images of discharged cathode showing Li_2O_2 deposited on MoS_2 cathode. c) STEM image of the cathode surface after the 10th discharge. d,e) EELS spectra of Li_2O_2 at the cathode surface after its 10th discharge; d) O–K edge and e) Li–K edge. f) XPS of the cathode including O 1s and Li 1s regions after the 10th discharge. g) XPS results of In3d region on the Li anode after the 10th cycle in ambient air. h) Top-view SEM-EDX composition mapping of anode for Indium element. i) EIS measurements and fitted data for fresh and cycled anode surface. The dots represent the experimental data and lines represent the fitted data.

porting Information). EELS is performed to further identify the elemental composition of the discharge product that is formed on the surface of the MoS_2 nanoflakes. A TEM micrograph of the sample used in this EELS analysis and the regions on this sample from which the EELS data are acquired are shown in Figure 3c. The Li K- and O K-edges obtained from these EELS measurements, which are attributed to a Li_2O_2 product, are presented in Figure 3d,e. The sharp Li K- and O K-edges in the spectra confirm the presence of these elements in the surface layer, and the dataset is also consistent with previously reported EELS measurements involving a Li_2O_2 product[32] (for the details of EELS experiment, see Section S4, Supporting Information). Furthermore, XPS was performed on the discharged cathode after 10th cycle. The presence of Li 1s and O 1s peaks at 56.0 and 532.5 eV, respectively, further confirms the Li_2O_2 as the discharge product on the cathode surface[46] (Figure 3f). Section S5 (Supporting Information) presents the XPS results of the cathode obtained in an oxygen environment.

To analyze the solid electrolyte interphase (SEI) layer on the Li anode. XPS was performed on the Li anode surface after 10th cycles of battery operation as shown in (Figure 3g). The main In 3d peaks were observed at 444.6 and 452.2 eV.[47] Two extra peaks were also located at 441.3 and 450.3 eV. These peaks suggest the formation of SEI layer on the anode containing In and Li-In alloy.[34] Scanning electron microscopy-energy dispersive X-ray spectroscopy (SEM–EDS) was conducted on the anode surface after 10th charge cycle as shown in (Figure 3h). The top view of SEM–EDS shows elemental mapping of indium revealing its presence and indicating the uniform layer formation on top of the anode. Electrochemical impedance spectroscopy (EIS) measurements were also conducted on the anode with different cycling (0, 5, 15, 20 cycles) as shown in (Figure 3i). Our results suggest the rise in the charge transfer resistance from 55 to 84 ohms after 20 cycles, indicating the formation of an SEI layer (for the details of EIS experiment see Section S6, Supporting Information).

To test the performance of our battery for the flexible and wearable applications, we probed its performance both with and without bending. **Figure 4**a demonstrates a similar OCV (open circuit voltage) obtained for the bent (3.00 V) and flat (3.04 V) conditions. The battery was also tested to power up a red light-emitting diode (LED) in flat and bending conditions (Figure 4a) indicating good structural integrity of the battery (see Video S1 for wearable feasibility, Supporting Information).

To study the effect of bending cycles on the performance of the battery, a fatigue bending test was performed in ambient air for 1000 cycles as shown in Figure 4b (for the details of fatigue bending test see Section S7, Supporting Information). A deep discharge experiment with a current density of 1 A g^{-1} was carried out on the battery before and after repetitive bending as shown in Figure 4c. An almost identical discharge capacity of 56 Ah g^{-1} was obtained before and after bending. A comparison of discharge capacity and current density of our flexible Li–O_2 battery in ambient air with other references based on the cut-off voltage of 2.5 V is illustrated in Figure 4d. These results

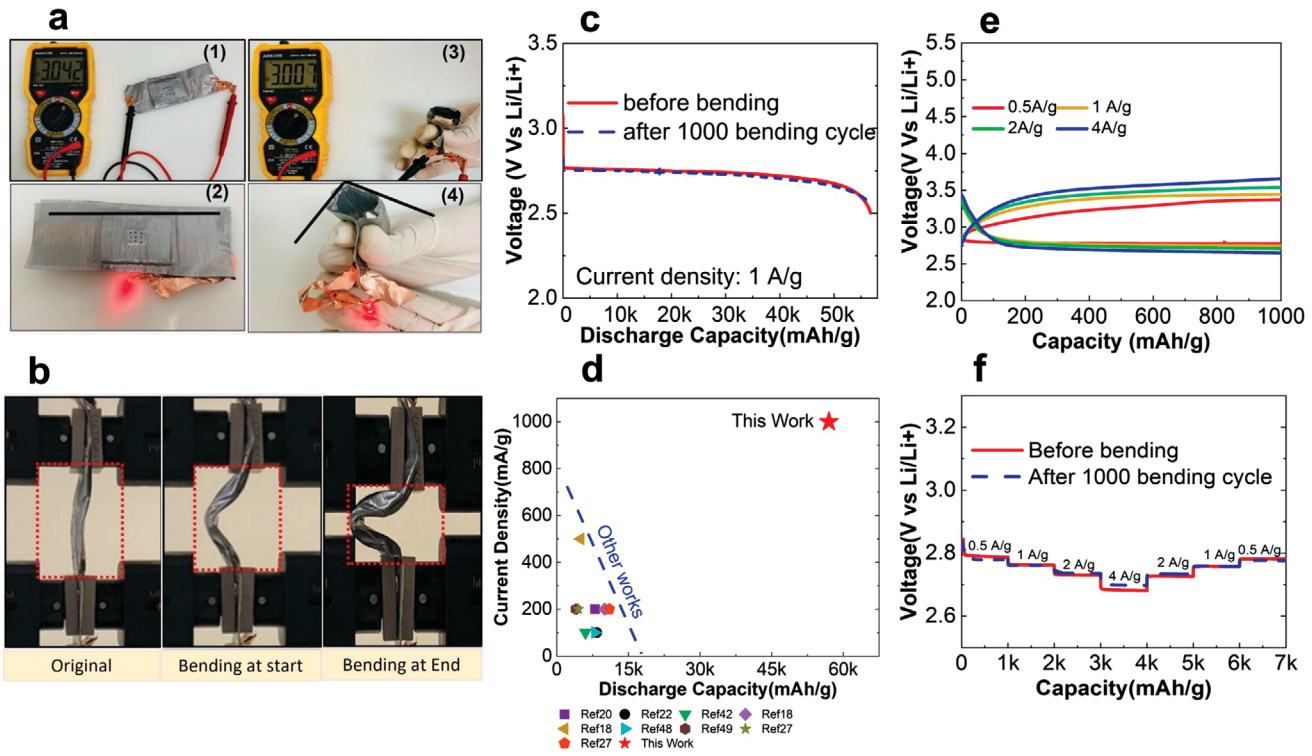

Figure 4. Bending test of flexible Li–O_2 battery in ambient air. a) Open circuit voltage measurement and LED lighting of flexible battery at different bending conditions; (1,2) flat (0° bending) and (3,4) bent batteries. b) Li–O_2 battery under bending experiment in ambient air (fatigue test). c) Deep discharge of flexible battery in ambient air before and after bending tests. d) Comparison of discharge capacity and current density of our battery in ambient air with other references based on cut-off voltage of 2.5 V. e) Charge/discharge curves at different current densities in ambient air. f) Rate capability results before and after bending test.

indicate that the performance (discharge capacity) of our flexible battery is significantly improved compared to the state-of-the-art results.[18,20,22,24,27,48,49] Figure 4e shows discharge–charge curves at different current densities of 0.5, 1, 2, and 4 A g^{-1} at a fixed capacity of 1000 mAh g^{-1}. The charge potential changes from 3.40 to 3.65 V upon increasing the current density from 0.5 to 4 A g^{-1}, indicating the effectiveness of our electrolyte blend in reducing the charge overpotential.

In addition, the rate capability of the battery was explored by increasing the discharge current density from 0.5 to 4 mA cm^{-2} and sweeping back to its initial value. As shown in Figure 4f, the potential difference after discharging up to 7 Ah g^{-1} capacity is negligible and the potential returns to the original value of ≈2.78 V. Moreover, the battery after 1000 bending cycles shows the same rate capability indicating an excellent structural and electrochemical integrity of the battery after bending tests.

3. Conclusions

In summary, we developed an air-breathing sheet-type flexible Li–O_2 battery operating under different conditions (oxygen, dry air, and ambient air). The flexible battery showed an excellent performance (370 cycles in pure oxygen, 250 cycles in dry air, and 240 cycles in ambient air) under a high current density of 1 A g^{-1}. It was uncovered that there is an excellent synergy between different components of the battery including electrolyte/redox mediator, cathode catalyst and Fomblin-based protection layer suppressing H_2O permeation into the battery cell. The battery operating in ambient air exhibited a superior performance including high charge/discharge curves stability, excellent rate capability and a deep-discharge capacity as high as 56 Ah/g before and after bending. The obtained results open a new direction in utilizing Li–O_2 batteries in flexible and wearable electronics.

4. Experimental Section

Materials: Lithium chips (>99.9%) were purchased from (MTI Corp), EMIM-BF4 (HPLC grade, >99.0%, Sigma-Aldrich), dimethyl sulfoxide (DMSO), Lithium Bis(trifluoromethanesulfonyl) imide (LiTFSI) (>99.0%), and MoS_2 powder were bought from (Sigma-Aldrich). Carbon cloth was obtained from (Fuel Cell Co.) and glass-fiber separator (WhatmanTM, GF/C) was acquired from GE healthcare science, Pressure-Sensitive Adhesive was procured from (Adhesive Research), polydimethylsiloxane (PDMS) was bought from (Gelpak Co) and heavy-duty duct tape was purchased from amazon.

Cathode Preparation: MoS_2 nanoflakes were prepared by liquid-phase exfoliation method. 300 mg of MoS_2 powder (99%) was dispersed in 60 mL isopropyl alcohol (>99.5%). The solution was then exfoliated using ultrasonication for 20 h followed by centrifugation at 2000 RPM for 1 h. The centrifuged MoS_2 was coated on top of the carbon cloth and then dried before use. The areal mass loading was 0.1 mg cm^{-2}.

Electrolyte Preparation: The electrolyte was prepared in argon-filled glove box. 1 M of Lithium LiTFSI) and 30×10^{-3} M of indium bromide ($InBr_3$) were added to the solution of DMSO and EMIM-BF4 ionic liquid with a volumetric ratio of 9–1, respectively.

Battery Assembly: For the battery assembly, the anode, separator, and cathode were stacked on top of each other. First, PDMS layer was attached via heavy-duty duct tape to a pressure-sensitive adhesive, followed by attaching to the copper sheet as a current collector. The polyethylene terephthalate spacer was then used to hold lithium anode. Second, the glass-fiber separator containing 50 µL of electrolyte was sandwiched between anode and MoS_2 coated carbon cloth cathode followed by attaching copper sheet. The membrane of carbon cloth used as a supporting matrix was soaked in the Fomblin liquid (oxygen permeable chemical), then assembled on the top of the cathode. Finally, another layer of PDMS was attached via heavy-duty tape (with punched holes) to allow air-breathing. The cell thickness and weight were measured to be 4 mm and 5 g, respectively. The whole assembly process was done in the argon-filled glove box with humidity and oxygen level less than 0.1 ppm. The galvanostatic tests were carried out inside small and sealed bags filled with pure oxygen or dry air. Other experiments were conducted in ambient air. Galvanostatic Battery analyzer (MTI Corp, BST8-MA) was used to run the battery experiments. All batteries were tested at room temperature (25 °C).

Supporting Information

Supporting Information is available from the Wiley Online Library or from the author.

Acknowledgements

A.S.-K., L.A.C., A.T.N., A.J., C.Z., acknowledge the support by the U.S. Department of Energy, Office of Energy Efficiency and Renewable Energy, Vehicle Technologies Office. L.M. and Z.H. acknowledge the support by NSF-DMREF (No. 1729420). A.S. and S.K.S. acknowledge support from NSF-CBET (award no. 1661038).

Conflict of Interest

The authors declare no conflict of interest.

Author Contributions

A.J. performed the battery tests and C.Z. helped with the analysis of results. A.J. carried out EIS experiment. A.S. and S.S performed TEM and EELS characterization. Z.H. and S.R. performed Raman and SEM characterization. S.W. performed SEM–EDS characterization. L.M. carried out XPS. M.D. and J.A. carried out the battery bending tests. L.A.C. and A.T.N. helped with the analysis of battery results. A.S.-K. supervised the battery experiments. All authors contributed to the manuscript writing.

Data Availability Statement

The data that support the findings of this study are available from the corresponding author upon reasonable request.

Keywords

energy storage, flexible battery, lithium air battery, lithium oxygen battery, molybdenum disulfide, redox mediator, wearable battery

Received: April 8, 2021
Revised: June 22, 2021
Published online: September 16, 2021

[1] C. Pang, J. H Koo, A. Nguyen, J. M. Caves, M.-G. Kim, A. Chortos, K. Kim, P. J. Wang, J. B.-H. Tok, Z. Bao, *Adv. Mater.* **2015**, *27*, 634.
[2] C. Dagdeviren, Y. Su, P. Joe, R. Yona, Y. Liu, Y. S. Kim, Y. Huang, A. R. Damadoran, J. Xia, L. W. Martin, Y. Huang, J. A. Rogers, *Nat. Commun.* **2014**, *5*, 4496.
[3] Y. Tai, Z. Yang, *Adv. Mater. Interfaces* **2017**, *4*, 1700496.
[4] X. Wang, Y. Gu, Z. Xiong, Z. Cui, T. Zhang, *Adv. Mater.* **2014**, *26*, 1336.
[5] G. Y. Bae, S. W. Pak, D. Kim, G. Lee, D. H. Kim, Y. Chung, K. Cho, *Adv. Mater.* **2016**, *28*, 5300.
[6] T. Q. Trung, S. Ramasundaram, B.-U. Hwang, N.-E. Lee, *Adv. Mater.* **2016**, *28*, 502.
[7] K. Sim, Z. Rao, Z. Zou, F. Ershad, J. Lei, A. Thukral, J. Chen, Q.-A. Huang, J. Xiao, C. Yu, *Sci. Adv.* **2019**, *5*, eaav9653.
[8] Y. H. Jung, T.-H. Chang, H. Zhang, C. Yao, Q. Zheng, V. W. Yang, H. Mi, M. Kim, S. J. Cho, D.-W. Park, H. Jiang, J. Lee, Y. Qiu, W. Zhou, Z. Cai, S. Gong, Z. Ma, *Nat. Commun.* **2015**, *6*, 7170.
[9] Q. Fu, Yi Chen, M. Sorieul, *ACS Nano* **2020**, *14*, 3528.
[10] J. Kang, D. Son, O. Vardoulis, J. Mun, N. Matsuhisa, Y. Kim, J. Kim, J. B.-H. Tok, Z. Bao, *Adv. Mater. Technol.* **2019**, *4*, 1800417.
[11] C. H. Lee, Y. Ma, K.-I. Jang, A. Banks, T. Pan, X. Feng, J. S. Kim, D. Kang, M. S. Raj, B. L. Mcgrane, B. Morey, X. Wang, R. Ghaffari, Y. Huang, J. A. Rogers, *Adv. Funct. Mater.* **2015**, *25*, 3698.
[12] J. Zhang, Y. Cao, M. Qiao, L. Ai, K. Sun, Q. Mi, S. Zang, Y. Zuo, X. Yuan, Qi Wang, *Sens. Actuators, A* **2018**, *274*, 132.
[13] N. Imanishi, A. C. Luntz, P. Bruce, *The Lithium Air Battery, Fundamentals*, Springer, New York **2014**.
[14] A. C. Luntz, B. D. Mccloskey, *Chem. Rev.* **2014**, *114*, 11721.
[15] D. Aurbach, B. D. Mccloskey, L. F. Nazar, P. G. Bruce, *Nat. Energy* **2016**, *1*, 16128.
[16] Q.-C. Liu, L. Li, J.-J. Xu, Z.-W. Chang, D. Xu, Y.-B. Yin, X.-Y. Yang, T. Liu, Y.-S. Jiang, J.-M. Yan, X.-B. Zhang, *Adv. Mater.* **2015**, *27*, 8095.
[17] H. Kim, H. Lee, M. Kim, Y. Bae, W. Baek, K. Park, S. Park, T. Kim, H. Kwon, W. Choi, K. Kang, S. Kwon, D. Im, *Carbon* **2017**, *117*, 454.
[18] Q.-C. Liu, J.-J. Xu, D. Xu, X.-B. Zhang, *Nat. Commun.* **2015**, *6*, 7892.
[19] X. Zou, Q. Lu, Y. Zhong, K. Liao, W. Zhou, Z. Shao, *Small* **2018**, *14*, 1801798.
[20] Q.-C. Liu, J.-J. Xu, Z.-W. Chang, D. Xu, Y.-B. Yin, X.-Y. Yang, T. Liu, Y.-S. Jiang, J.-M. Yan, X.-B. Zhang, *Part. Part. Syst. Charact.* **2016**, *33*, 500.
[21] H. Xue, S. Wu, J. Tang, H. Gong, P. He, J. He, H. Zhou, *ACS Appl. Mater. Interfaces* **2016**, *8*, 8427.
[22] X.-Y. Yang, J.-J. Xu, D. Bao, Z.-W. Chang, D.-P. Liu, Y. Zhang, X.-B. Zhang, *Adv. Mater.* **2017**, *29*, 1700378.
[23] C. Chen, S. Xu, Y. Kuang, W. Gan, J. Song, G. Chen, G. Pastel, B. Liu, Y. Li, H. Huang, L. Hu, *Adv. Energy Mater.* **2019**, *9*, 1802964.
[24] Q.-C. Liu, T. Liu, D.-P. Liu, Z.-J. Li, X.-B. Zhang, Y. Zhang, *Adv. Mater.* **2016**, *28*, 8413.
[25] T. Liu, J.-J. Xu, Q.-C. Liu, Z.-W. Chang, Y.-B. Yin, X.-Y. Yang, X.-B. Zhang, *Small* **2017**, *13*, 1602952.
[26] L. Wang, Y. Zhang, J. Pan, H. Peng, *J. Mater. Chem. A* **2016**, *4*, 13419.
[27] C. Shu, J. Long, S.-X. Dou, J. Wang, *Small* **2019**, *15*, 1804701.
[28] Y. Jiang, J. Cheng, Lu Zou, X. Li, Y. Huang, L. Jia, B. Chi, J. Pu, J. Li, *ChemCatChem* **2017**, *9*, 4231.
[29] A. C. Luntz, B. D. Mccloskey, *Nat. Energy* **2017**, *2*, 17056.
[30] Z. Guo, C. Li, J. Liu, Y. Wang, Y. Xia, *Angew. Chem.* **2017**, *129*, 7613.
[31] X. B. Zhu, T. S. Zhao, Z. H. Wei, P. Tan, L. An, *Energy Environ. Sci.* **2015**, *8*, 3745.
[32] M. Asadi, B. Sayahpour, P. Abbasi, A. T. Ngo, K. Karis, J. R. Jokisaari, C. Liu, B. Narayanan, M. Gerard, P. Yasaei, X. Hu, A. Mukherjee, K. C. Lau, R. S. Assary, F. Khalili-Araghi, R. F. Klie, L. A. Curtiss, A. Salehi-Khojin, *Nature* **2018**, *555*, 502.
[33] M. Xie, Z. Huang, X. Lin, Y. Li, Z. Huang, L. Yuan, Y. Shen, Y. Huang, *Energy Storage Mater.* **2019**, *20*, 307.
[34] J. Liu, T. Wu, S. Zhang, D. Li, Y. Wang, H. Xie, J. Yang, G. Sun, *J. Power Sources* **2019**, *439*, 227095.
[35] X. Lin, T. Zhang, C. Chu, Z. Li, R. Liu, P. Li, Yi Li, Z. Huang, Y. Ma, *ACS Sustainable Chem. Eng.* **2020**, *8*, 7581.
[36] X. Lin, Q. Kang, Z. Zhang, R. Liu, Y. Li, Z. Huang, X. Feng, Y. Ma, W. Huang, *J. Mater. Chem. A* **2017**, *5*, 3638.
[37] A. Kondori, Z. Jiang, M. Esmaeilirad, M. Tamadoni Saray, A. Kakekhani, K. Kucuk, P. Navarro Munoz Delgado, S. Maghsoudipour, J. Hayes, C. S. Johnson, C. U. Segre, R. Shahbazian-Yassar, A. M. Rappe, M. Asadi, *Adv. Mater.* **2020**, *32*, 2004028.
[38] H. Wang, F. Yin, N. Liu, H. Yu, T. Fan, B. Chen, *ACS Sustainable Chem. Eng.* **2021**, *9*, 4509.
[39] J. Li, H. Zhou, Z. Jian, H. Li, X. Guan, Y. Xing, S. Zhang, H. Xu, *ACS Sustainable Chem. Eng.* **2021**, *9*, 5334.
[40] J. Zhang, X. Luo, X. Li, Q. Yang, J. He, S. Xin, X. Yang, Y. Yu, D. Zhang, C. Zhang, *ChemElectroChem* **2021**, *8*, 949.
[41] M. Asadi, B. Kumar, C. Liu, P. Phillips, P. Yasaei, A. Behranginia, P. Zapol, R. F. Klie, L. A. Curtiss, A. Salehi-Khojin, *ACS Nano* **2016**, *10*, 2167.
[42] S. Rastegar, Z. Hemmat, C. Zhang, S. Plunkett, J. Wen, N. Dandu, T. Rojas, L. Majidi, S. N. Misal, A. T. Ngo, L. A. Curtiss, A. Salehi-Khojin, *ACS Appl. Mater. Interfaces* **2021**, *13*, 4915.
[43] C. Zhang, N. Dandu, S. Rastegar, S. N. Misal, Z. Hemmat, A. T. Ngo, L. A. Curtiss, A. Salehi-Khojin, *Adv. Energy Mater.* **2020**, *10*, 2000201.
[44] Y. Liu, Y. Zang, X. Liu, J. Cai, Z. Lu, S. Niu, Z. Pei, T. Zhai, G. Wang, *Front. Energy Res.* **2020**, *8*, 109.
[45] A. Hu, C. Shu, X. Qiu, M. Li, R. Zheng, J. Long, *ACS Sustainable Chem. Eng.* **2019**, *7*, 6929.
[46] K. N. Wood, G. Teeter, *ACS Appl. Energy Mater.* **2018**, *1*, 4493.
[47] T. Zhang, K. Liao, P. He, H. Zhou, *Energy Environ. Sci.* **2016**, *9*, 1024.
[48] T. Liu, X.-L. Feng, X. Jin, M.-Z. Shao, Y.-T. Su, Y. Zhang, X.-B. Zhang, *Angew. Chem.* **2019**, *131*, 18408.
[49] T. Liu, Q.-C. Liu, J.-J. Xu, X.-B. Zhang, *Small* **2016**, *12*, 3101.